1724 *Chem. Mater.* **2010,** *22,* 1724–1731
DOI:10.1021/cm903146x

CHEMISTRY OF MATERIALS
Article

Properties of Fluorenyl Silanes in Organic Light Emitting Diodes

Wei Wei, Peter I. Djurovich, and Mark E. Thompson*

Department of Chemistry, University of Southern California, Los Angeles 90089-0744

Received October 12, 2009. Revised Manuscript Received December 27, 2009

Multifluorenyl silanes have been studied as potential hosts for organic light emitting diodes. Four molecules, (9,9′-dimethylfluoren-2-yl)$_n$Si(phenyl)$_{4-n}$ (**SiFln**, n = 1, 2, 3, and 4), with an increasing number of fluorene units have been synthesized and investigated. These compounds possess high triplet energies (2.9 eV), large HOMO−LUMO gaps (~5.2 eV), and high glass transition temperatures. Their glass transition and sublimation temperatures increase linearly as the fluorene ratio increases, but there are only small changes in their electrochemical or photophysical properties. These studies suggest that the Si center helps maintain the high singlet and triplet energy levels of these molecules. These materials exhibit ambipolar transport characteristics in undoped OLED devices, and the charge conductivity of the devices was enhanced by increasing the fluorene ratios in the host molecules. Compared with phenylsilanes, the fluorenylsilanes show better hole injecting and charge transporting abilities. **SiFl4** was investigated as a host material for red, green, and blue phosphorescent devices, giving peak efficiencies of 8, 8, and 3%, respectively.

Introduction

Ever since the doping strategy has been developed to prevent self-quenching of the emissive molecules, the technique has been widely utilized to optimize the efficiencies of organic light emitting diode (OLED) devices.[1] Typical doped OLED devices consist of several discrete molecular or polymeric layers: an electron transport layer (ETL), an emissive layer (EML), and a hole transport layer (HTL). While the ETL and HTL are used to inject and transport electrons and holes into the EML, the EML is where the charges recombine and form the dopant (emissive molecule) excitions. In a doped device, a host material is also employed in the EML to inhibit self-quenching by the dopant and to confine the energy on the dopant molecules. The host plays an important role in an OLED device because its energy levels and charge mobilities determine 1) whether the holes and electrons recombine at the emissive layer and 2) whether the emission can be confined into the dopant exclusively. The host material used in an OLED thus has to be energetically matched with a specific dopant. The most common hosts for OLEDs are carbazole derivatives, i.e. *N,N*′-dicarbazolyl-3,5-benzene (mCP)[2−4] and 4, 4′-*N,N*′-dicarbazole-biphenyl (CBP).[2,5,6] However, carbazoles have relatively low glass transition temperatures (T_g) and have been shown to be chemically unstable in the devices, which can ultimately lead to a shortened device lifetimes.[7,8] Compounds that have large energy band gaps and contain no easily oxidized nitrogen donor groups, bis(triphenylsilyl)-benzenes, have been developed as host materials, particularly for blue phosphorescent emitters.[9−13] Unfortunately, these materials have low glass transition temperatures, and the deep energy level of their HOMOs hinder hole injection into heterojunction devices. Therefore, further investigations are still needed to develop host materials that can improve the performance of OLEDs.

Fluorene derivatives have been studied in OLEDs due to their robust thermal stability, high charge transport mobilities, large HOMO−LUMO gaps, and relatively high T_gs.[14−17] Spirobifluorene oligomers (**Fln**, Scheme 1) have excellent

*Corresponding author e-mail: met@usc.edu.

(1) Tang, C. W.; Van Slyke, S. A. *Appl. Phys. Lett.* **1987**, *51*, 9131.
(2) Holmes, R. J.; Forrest, S. R.; Tung, Y. J.; Kwong, R. C.; Brown, J. J.; Garon, S.; Thompson, M. E. *Appl. Phys. Lett.* **2003**, *82*, 2422.
(3) D'Andrade, B. W.; Forrest, S. R. *J. Appl. Phys.* **2003**, *94*, 3101.
(4) Holmes, R. J.; Forrest, S. R.; Sajoto, T.; Tamayo, A.; Djurovich, P. I.; Thompson, M. E. *Org. Electron.* **2006**, *7*, 163.
(5) O'Brien, D. F.; Baldo, M. A.; Thompson, M. E.; Forrest, S. R. *Appl. Phys. Lett.* **1999**, *74*, 442.
(6) Baldo, M. A.; Lamansky, S.; Burrows, P. E.; Thompson, M. E.; Forrest, S. R. *Appl. Phys. Lett.* **1999**, *75*, 4.
(7) Scholz, S.; Corten, C.; Walzer, K.; Kuckling, D.; Leo, K. *Org. Electron.* **2007**, *8*, 709.
(8) Kondakov, D. Y.; Lenhart, W. C.; Nichols, W. F. *J. Appl. Phys.* **2007**, *101*, 024512.
(9) Holmes, R. J.; Forrest, S. R.; Sajoto, T.; Tamayo, A.; Djurovich, P. I.; Thompson, M. E.; Brooks, J.; Tung, Y. J.; D'Andrade, B. W.; Weaver, M. S.; Kwong, R. C.; Brown, J. J. *Appl. Phys. Lett.* **2005**, *87*, 243507.
(10) Kanno, H.; Sun, Y.; Forrest, S. R. *Appl. Phys. Lett.* **2005**, *86*, 263502.
(11) Ren, X. F.; Li, J.; Holmes, R. J.; Djurovich, P. I.; Forrest, S. R.; Thompson, M. E. *Chem. Mater.* **2004**, *16*, 4743.
(12) Holmes, R. J.; D'Andrade, B. W.; Forrest, S. R.; Ren, X.; Li, J.; Thompson, M. E. *Appl. Phys. Lett.* **2003**, *83*, 3818.
(13) Sun, Y. r.; Forrest, S. R. *Appl. Phys. Lett.* **2007**, *91*, 263503.
(14) Wu, C. C.; Liu, T. L.; Hung, W. Y.; Lin, Y. T.; Wong, K. T.; Chen, R. T.; Chen, Y. M.; Chien, Y. Y. *J. Am. Chem. Soc.* **2003**, *125*, 3710.
(15) Chen, L. Y.; Ke, T. H.; Wu, C. C.; Chao, T. C.; Wong, K. T.; Chang, C. C. *Appl. Phys. Lett.* **2007**, *91*, 163509.
(16) Wu, C. C.; Liu, W. G.; Hung, W. Y.; Liu, T. L.; Lin, Y. T.; Lin, H. W.; Wong, K. T.; Chien, Y. Y.; Chen, R. T.; Hung, T. H.; Chao, T. C.; Chen, Y. M. *Appl. Phys. Lett.* **2005**, *87*, 052103.
(17) Wu, C. I.; Lee, G. R.; Lin, C. T.; Chen, Y. H.; Hong, Y. H.; Liu, W. G.; Wu, C. C.; Wong, K. T.; Chao, T. C. *Appl. Phys. Lett.* **2005**, *87*, 242107.

 Published on Web 01/12/2010

Scheme 1

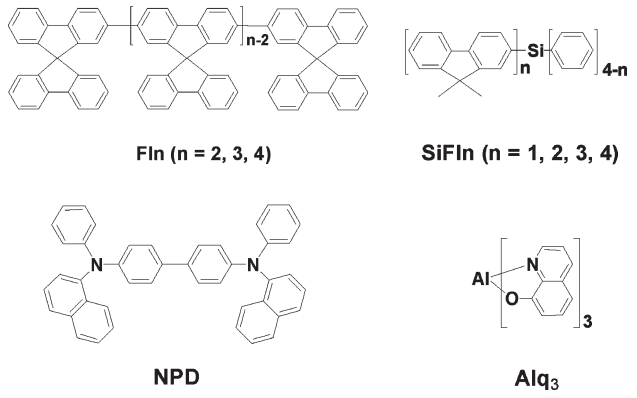

thermal and chemical stabilities as well as high charge transport mobilities ($\mu = 10^{-5}-10^{-3}$ cm^2/V·s) for both holes and electrons.[14−17] Mobilities for the conjugated **Fln** oligmers are comparable to one of the most common OLED hole transporters, NPD (Scheme 1), and 2 orders of magnitude better than the common OLED electron transporter Alq_3 (Scheme 1).[18,19] Wu et al. found that the number of the fluorene units in the oligomer is inversely correlated with the charge transport mobility of the molecule; as the number decreased from four to two, the charge carrier mobility increased.[19] While the data reported by Wu et al. suggested that the best properties would be found for simple monofluorenes, this idea could not be investigated due to the high volatility of such low molecular weight species. Monofluorene containing materials with low volatility, such as triphenyl-(4-(9-phenyl-9H-fluoren-9-yl)phenyl)silane (TPSi-F),[20] have been reported; however, variants of this molecule with increased fluorene content have not been examined.

In order to explore the properties of monofluorenylated materials in OLEDs, we have chosen to study compounds with multiple-linked, nonconjugated fluorenes. The materials examined here are fluorenylsilanes, **SiFln**, n = 1, 2, 3, 4 (Scheme 1). While the use of arylsilanes in OLEDs has been previously reported,[9−13,20,21] these compounds have not been used to assemble multiple fluorenes into a single molecule as described here. The fluorenes in the molecules presented here are electronically isolated, leading to a high triplet energy and large HOMO/LUMO gap. These materials have high glass transition temperatures and show ambipolar charge transport characteristics, making them promising host materials for OLED devices.

Experimental Section

General. All chemicals, reagents, and solvents were received from commercial sources without further purification except for tetrahydrofuran (THF) that had been distilled over sodium/benzophenone. All glassware used was oven-dried, and the reactions were performed under N_2.

Scheme 2

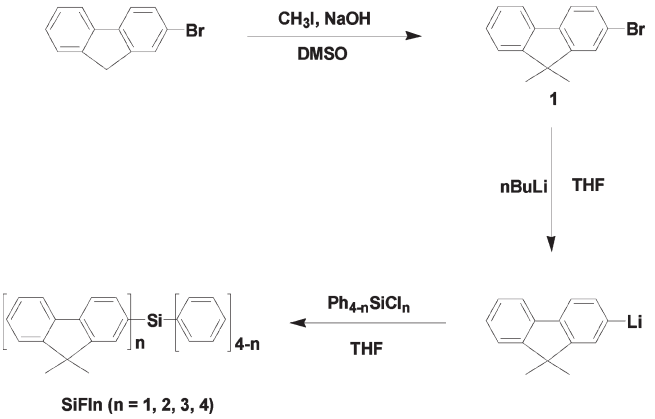

Procedures. 2-Bromo-9,9′-dimethylfluorene (**1**, Scheme 2) was synthesized according to literature procedures.[22,23] The fluorenylsilanes were synthesized as shown in Scheme 2, according to the literature reported conditions.[24,25] To a solution of **1** (C_1 = 0.25 M) in anhydrous THF, 1.2 equiv of nBuLi (2.5 M in hexanes) was added dropwise at −78 °C. The reaction mixture was allowed to warm up to room temperature, and the corresponding phenylchlorosilane ($Ph_{4-n}SiCl_n$, n = 1, 2, 3 and 4, 1/n eq., Scheme 2) was added dropwise after 1 h. The reaction mixture was stirred at room temperature overnight. The organic layer was extracted by ethyl acetate, washed with brine, and dried over magnesium sulfate. The resulted solution was evaporated to dryness under reduced pressure to give the crude products. Silica gel column chromatography with pentane and ethyl acetate (10:1) was performed to obtain white solids of the pure products.

2-Bromo-9, 9-dimethylfluorene (**1**) (Yield 94%): ^{1}H NMR ($CDCl_3$, 250 MHz): δ (ppm) 7.73−7.68(m, 2H), 7.60−7.56 (m, 2H), 7.48−7.32 (m, 3H), 1.48 (s, 6H).

SiFl1. Triphenyl-(9,9′-dimethylfluoren-2-yl)silane (Yield 92%): ^{1}H NMR ($CDCl_3$, 250 MHz): δ (ppm) 7.56−7.81 (m, 10H), 7.41 −7.52 (m, 10H), 7.32−7.41 (m, 2H), 1.48 (s, 6H). EIMS (*m*/z, %): 452 (M-1,100). Anal. Calcd. for $C_{33}H_{28}Si$: C, 87.56; H, 6.23. Found: C, 87.45; H, 6.23.

SiFl2. Diphenyldi(9,9′-dimethylfluoren-2-yl)silane (Yield 67%): ^{1}H NMR ($CDCl_3$, 250 MHz): δ (ppm) 7.54−7.80 (m, 12H), 7.39 −7.50 (m, 8H), 7.30−7.39 (m, 4H), 1.44 (s, 12H). EIMS (*m*/z, %): 568 (M-1,87). Anal. Calcd. for $C_{42}H_{36}Si$: C, 88.68; H, 6.38. Found: C, 88.65; H, 6.37.

SiFl3. Phenyltri(9,9′-dimethylfluoren-2-yl)silane (Yield 58%): ^{1}H NMR ($CDCl_3$, 250 MHz): δ (ppm) 7.58−7.80 (m, 14H), 7.40 −7.49 (m, 6H), 7.30−7.39 (m, 6H), 1.45 (s, 18H). EIMS (*m*/z, %): 684 (M-1,36). Anal. Calcd. for $C_{51}H_{44}Si$: C, 89.43; H, 6.47. Found: C, 89.45; H, 6.45.

SiFl4. Tetra(9,9′-dimethylfluoren-2-yl)silane (Yield 52%): ^{1}H NMR ($CDCl_3$, 250 MHz): δ (ppm) 7.61−7.81 (m, 16H) 7.40 −7.47 (m, 4H), 7.30−7.39 (m, 8H), 1.46 (s, 24H). EIMS

(18) Kepler, R. G.; Beeson, P. M.; Jacobs, S. J.; Anderson, R. A.; Sinclair, M. B.; Valencia, V. S.; Cahill, P. A. *Appl. Phys. Lett.* **1995**, *66*, 3618.
(19) Wu, C. C.; Liu, T. L.; Lin, Y. T.; Hung, W. Y.; Ke, T. H.; Wong, K. T.; Chao, T. C. *Appl. Phys. Lett.* **2004**, *85*, 1172.
(20) Shih, P. I.; Chien, C. H.; Chuang, C. Y.; Shu, C. F.; Yang, C. H.; Chen, J. H.; Chi, Y. *J. Mater. Chem.* **2007**, *17*, 1692.
(21) Tsai, M. H.; Lin, H. W.; Su, H. C.; Ke, T. H.; Wu, C. C.; Fang, F. C.; Liao, Y. L.; Wong, K. T.; Wu, C. I. *Adv. Mater.* **2006**, *18*, 1216.
(22) Zhan, X. W.; Risko, C.; Amy, F.; Chan, C.; Zhao, W.; Barlow, S.; Kahn, A.; Bredas, J. L.; Marder, S. R. *J. Am. Chem. Soc.* **2005**, *127*, 9021.
(23) Xie, N.; Zeng, D. X.; Chen, Y. *Synlett* **2006**, *5*, 737.
(24) Liao, Y.; Baskett, M.; Lahti, P. M.; Palacio, F. *Chem. Commun.* **2002**, 252.
(25) You, Y.; An, C. G.; Kim, J. J.; Park, S. Y. *J. Org. Chem.* **2007**, *72*, 6241.

(*m*/z, %): 607 (M-$C_{15}H_{13}$,48). Anal. Calcd. for $C_{60}H_{52}Si$: C, 89.95; H, 6.54. Found: C, 89.91; H, 6.47.

Differential Scanning Calorimetry. Differential scanning calorimetry (DSC) was performed using a TA Instruments DSC Q10 instrument with a scanning range from room temperature to 300 °C. The sample was first scanned at a heating rate of 10 °C min^{-1} and was cooled down to room temperature rapidly using liquid N_2. The second and third scans were performed at a heating rate of 5 °C min^{-1}. The glass transition temperatures were determined from either the second or the third scan for each compound.

Electrochemistry and Photophysics. Cyclic voltammetry (CV) and differential pulse voltammetry (DPV) were performed using an EG&G potentiostat/galvanostat model 283 under N_2 atmosphere. Anhydrous DMF was used as solvent for the scan from −3.7 to 1.0 V to detect the reduction signals, while anhydrous acetonitrile was used as a solvent for the scan from −0.5 to 2.5 V to detect the oxidation signals, and 0.1 M tetrabutylammonium hexafluorophosphate (TBAH) was used as the supporting electrolyte. A glassy carbon rod was used as the working electrode, a platinum wire was used as the counter electrode, and a silver wire was used as a pseudoreference electrode. The reversibility and the redox potentials were determined by the cyclic voltammetry and differential pulse voltammetry, respectively. The redox potentials were calculated relative to an internal reference ferrocenium/ferrocene (Cp_2Fe^+/Cp_2Fe). The UV−visible spectra were measured in dichoromethane using a Hewlett-Packard 4853 diode array spectrometer. Steady state emission measurements of both solutions and thin films were performed at room temperature and 77 K using a Photon Technology International (PTI) QuantaMaster model C-60 fluorimeter. Room temperature emission lifetimes were measured using an IBH Fluorocube instrument equipped with a 281 nm diode excitation source. Low temperature phosphorescent lifetimes of thin films were measured using a PTI QuantaMaster fluorimeter on samples immersed in liquid nitrogen.

Device Fabrication. All materials used for vapor deposition were purified by temperature gradient vacuum sublimation. Indium tin oxide (ITO) on glass was provided by Thin Film Devices Inc. ITO substrates were cleaned by detergent, rinsed with deionized water, sonicated in organic solvents (tetrachloroethylene, acetone, and ethanol), and finally treated with UV ozone for 10 min. The organics were vapor-deposited onto the substrates in a high-vacuum chamber, followed by the LiF (10 Å) and the aluminum cathode (1000 Å) deposition using a shadow mask with 2-mm wide stripes. The electrical and optical characteristics of the devices were measured with a Keithly 2400 source/meter/2000 multimeter coupled to a Newport 1835-C optical meter, equipped with a UV 818 Si photo detector. The electroluminescence (EL) spectra were measured on a Photon Technology International QuantaMaster model C-60 fluorimeter.

Result and Discussion

Design, Synthesis, and Characterization of the Molecules. The molecular structures of the four fluorenylsilanes **SiFln** (n = 1, 2, 3, 4) were specifically designed to achieve a high level of fluorene incorporation in the molecules, while keeping them electronically isolated to prevent the red shift associated with conjugated oligo- and polyfluorenes. Tetraarylsilanes were chosen for their thermal stability, relatively high T_gs, and the flexibility for structural modification.[26−28] The synthetic approach and structures of the **SiFln** compounds are shown in Scheme 2. The compounds were synthesized using a lithium-halogen exchange reaction of 2-bromo-9,9′-dimethylfluorene with n-butyllithium, followed by the addition of phenylchlorosilane to the lithiated fluorene, in good-to-excellent yields (52−92%).[24,25] The yields decreased as the number of fluorenyl groups in the molecule is increased, presumably due to steric hindrance that slows the rate of addition of each successive fluorenyl group to the silyl center.

Table 1. Thermal Properties of SiFln

n	1	2	3	4
T_g (°C)[a]	45	76	103	126
T_{sub} (°C)[b]	179	222	245	302

[a] Measured by differential scanning calorimetry. [b] Measured by gradient vacuum sublimation at 5×10^{-6} Torr.

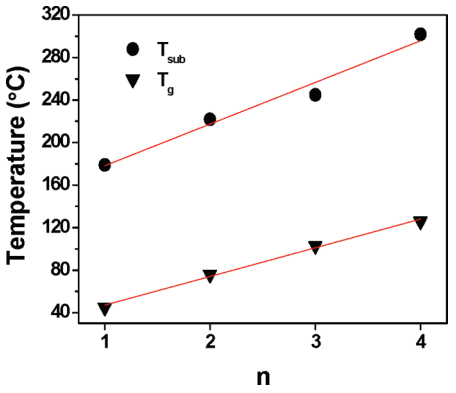

Figure 1. Dependence of the glass transition temperature, T_g (triangle), and the sublimation temperature, T_{sub} (circle), on the number of fluorenes in **SiFln**.

Thermal Properties. Amorphous materials with high glass transition temperatures are beneficial for OLEDs since crystallization can introduce deleterious grain boundaries in homogeneous films. The glass transition temperature of the molecules is related to their molecular structures.[29−32] The **SiFln** compounds have been designed to possess high glass transition temperatures because 1) they have symmetrical tetrahedral structures, 2) they have relatively high molecular weights, and 3) they contain rigid and bulky aromatic groups. The glass transition temperatures of the fluorenyl silanes were measured using differential scanning calorimetry (DSC). Samples were rapidly cooled from a melt after the first DSC scan to obtain glassy materials. Glass transition temperatures for all four materials were clearly observed on subsequent second and third scans (Table 1). The values for **SiFl2**, **SiFl3**, and **SiFl4**

(26) Uchida, M.; Izumizawa, T.; Nakano, T.; Yamaguchi, S.; Tamao, K.; Furukawa, K. *Chem. Mater.* **2001**, *13*, 2680.
(27) Chan, L. H.; Lee, R. H.; Hsieh, C. F.; Yeh, H. C.; Chen, C. T. *J. Am. Chem. Soc.* **2002**, *124*, 6469.
(28) Yu, G.; Xu, X.; Liu, Y.; Jiang, Z.; Yin, S.; Shuai, Z.; Zhu, D. *Appl. Phys. Lett.* **2005**, *87*, 222115.
(29) Shirota, Y. *J. Mater. Chem.* **2000**, *10*, 1.
(30) Shirota, Y. *J. Mater. Chem.* **2005**, *15*, 75.
(31) O'Brien, D. F.; Burrows, P. E.; Forrest, S. R.; Koene, B. E.; Loy, D. E.; Thompson, M. E. *Adv. Mater.* **1998**, *10*, 1108.
(32) Koene, B. E.; Loy, D. E.; Thompson, M. E. *Chem. Mater.* **1998**, *10*, 2235.

Table 2. Electrochemical and Photophysical Characteristics of SiFln

n	E_{ox}[a] (V)	E_{red}[b] (V)	$\lambda_{abs,\ solution}$[c] λ, nm (ε, 10^5 cm^{-1} M^{-1})	$\lambda_{max,PL,\ solution}$[d] (nm)	τ_{film}[e] ns (λ, nm)[f]	τ_{film}[e] ms (λ, nm)[g]
1	1.4	−2.8	307 (1.32)	310, 434	2.7 (431)	700 (512)
2	1.4	−2.9, −3.1	308 (0.75)	312, 436	2.5 (417)	740 (510)
3	1.4	−2.9, −3.1, −3.3	309 (0.56)	312, 436	2.5 (409)	840 (505)
4	1.4	−3.1, −3.3, −3.5	310 (0.26)	310, 436	2.4 (431)	730 (513)

[a] In anhydrous acetonitrile. [b] In anhydrous DMF. [c] In CH_2Cl_2. [d] 10^{-5} M in 2-methyl THF. The first value is for fluorescence measured at room temperature, the second value is for phosphorescence measured at 77 K. [e] By organic vapor phase deposition. [f] Fluorescence measured at room temperature. [g] Phosphorescence measured at 77 K

range from 76−126 °C (see Table 1, Figure 1, and Figure S1 in the Supporting Information) and exceed those of bis-(triphenylsilyl)benzenes[11] (26−53 °C), mCP (65 °C), and CBP (60 °C). For example, **SiFl2** has a molecular weight similar to that of 1,3-bis(triphenylsilyl)benzene (UGH3), yet the former has a glass transition temperature that is 30 °C higher. A linear relationship found between the number of fluorenyl groups in the molecule and the glass transition temperature (Figure 1) supports our prediction that fluorenyl groups act to stabilize the glassy states of these tetraarylsilanes. Another important characteristic of these fluorene based materials, with respect to OLED fabrication, is their high sublimation temperatures, which range from 179 to 302 °C at 5×10^{-6} torr (Table 1 and Figure 1). The sublimation temperature also increases with the increasing fluorene content in the **SiFln** molecules, similar to the trend observed for the T_g values.

Electrochemistry. The electrochemical properties of these compounds were studied by cyclic voltammetry (CV) and differential pulse voltammetry (DPV). The reduction and oxidation potentials of these molecules versus Cp_2Fe^+/Cp_2Fe are listed in Table 2. Reversible reduction waves were observed for all four compounds, with first reduction potentials observed at −2.8 to −3.1 V (Figure 2 and Figure S2). Multiple waves were observed for **SiFl2**, **SiFl3**, and **SiFl4** corresponding to the reduction of each fluorenyl moiety in the molecule (Figure S2). The fourth reduction of **SiFl4** was not observed, as it is presumably obscured by solvent reduction. The shift to higher potential for the first reduction process as the number of fluorene groups increases suggests that weak electronic coupling occurs between the individual fluorene units.

Oxidation waves for the **SiFln** compounds occur at ∼1.4 eV and are irreversible, as shown in Figure 2 for **SiFl4**. The absence of a reversible couple leads to some ambiguity as to whether the measured potential represents the thermodynamic value for oxidation process. Rathore et al. investigated a series of π-stacked, nonconjugated oligofluorenes that undergo reversible electrochemical oxidation and showed a linear correlation exists between the oxidation potential and the number of fluorene units in the chain, giving progressively higher oxidation potentials for shorter chains.[33] Even though oxidation of the fluorenyl group is irreversible in the **SiFln** compounds, the observed potential fits the

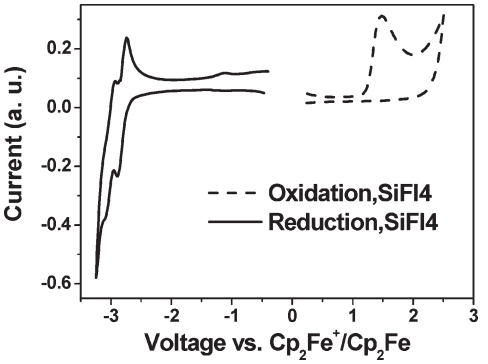

Figure 2. Cyclic voltammetric redox curves for **SiFl4**.

length-potential correlation of oligofluorenes found by Rathore. Therefore, we consider that, for the fluorenylsilanes reported here, the irreversible oxidation wave provides a valid estimate of the thermodynamic oxidation potential.

In order to design efficient OLEDs, it is important to determine the HOMO and LUMO energies of a new compound so that appropriate transport materials can be selected to match the energetic requirements for carrier injection and transport throughout the device. The HOMO and LUMO levels of all the molecules were determined using both density functional theory (DFT) and electrochemical experimental data. While DFT calculations do not give a direct measure of the HOMO or LUMO energy of the neat material, they are useful for predicting the sites of oxidation and reduction for each molecule. DFT calculations for the fluorenylsilanes show HOMO/LUMO orbitals and triplet surfaces primarily localized on the fluorenyl groups (see Figure S3). The calculated energies of the frontier orbitals are −5.64 eV to −5.75 eV for HOMOs and −0.96 eV to −1.04 eV for LUMOs.

Electrochemical methods have been commonly used to determine molecular frontier orbital energy levels.[34] The HOMO energies can be estimated from the correlation between the ultraviolet photoemission spectroscopy (UPS) measured HOMO energy and the oxidation potential of the molecule (eq 1),[34] while the LUMOs can be estimated from the correlation between the inverse photoelectron spectroscopy (IPES) measured LUMO energy and the reduction potential (eq 2).[35] A correlation

(33) Rathore, R.; Abdelwahed, S. H.; Guzei, I. A. *J. Am. Chem. Soc.* **2003**, *125*, 8712.
(34) D'Andrade, B. W.; Datta, S.; Forrest, S. R.; Djurovich, P.; Polikarpov, E.; Thompson, M. E. *Org. Electron.* **2005**, *6*, 11.
(35) Djurovich, P. I.; Mayo, E. I.; Forrest, S. R.; Thompson, M. E. *Org. Electron.* **2009**, *10*, 515.

between the LUMO levels calculated using DFT methods and the IPES measured LUMO energies has also been reported (eq 3).[35]

$$E_{HOMO} = -(1.4 \pm 0.1)E_{ox} - (4.6 \pm 0.08) \quad (1)$$

$$E_{LUMO} = -(1.19 \pm 0.08)E_{red} - (4.78 \pm 0.17) \quad (2)$$

$$E_{LUMO} = (0.92 \pm 0.04)E_{DFT\ LUMO} - (0.44 \pm 0.11) \quad (3)$$

Here, E_{HOMO} and E_{LUMO} are the HOMO and LUMO energies in eV, E_{ox} and E_{red} are the oxidation and reduction potentials in V, and $E_{DFT\ LUMO}$ is the LUMO energy calculated using DFT at the B3LYP level using either 6-31G* (hydrocarbons) or LACVP** (organometallics) basis sets (Titan v1.0.7, Wavefunction, Inc.).

Using the UPS/HOMO correlation, the HOMO energies are determined to be −6.6 eV for all the fluorenylsilanes. Using the IPES/LUMO correlation, the LUMO energies are estimated to be −1.4 eV for **SiFl1**, −1.3 eV for **SiFl2** and **SiFl3**, and −1.1eV for **SiFl4**. A similar LUMO energy (−1.3 eV) is obtained from the IPES/DFT LUMO correlation. Transport gaps of ca. 5.2 eV were calculated from the difference between the LUMO and HOMO energies. An optical gap energy of 4.0 eV was estimated from the long wavelength edge of the absorption spectra of the fluorenylsilanes. These two values fit well into the correlation found for the optical gap and the transport gap of related organic semiconductors.[35] The HOMO and LUMO levels of other molecules used for the OLED fabrications in this paper were determined using the same methodology.

Photophysics. The **SiFln** compounds were analyzed by UV−visible absorption and emission spectroscopy, and data and spectra are shown in Table 2 and Figure 3. The lowest-energy absorption transitions of all the fluorenylsilanes are close to 310 nm and show little shift in energy as a function of the number of fluorene groups (Figure 3a). The absorptivity in the region from 250 to 320 nm increases monotonically with the number of fluorene groups in the molecule, as expected for noninteracting chromophores. Fluorescence was observed for all of the compounds in dilute solution, with very small Stokes shifts from the lowest absorption bands (Table 2, Figure 3b). All of the **SiFln** compounds show phosphorescence at low temperatures (λ_{max} of 435 nm, Table 2, Figure 3c) corresponding to a triplet energy of 2.9 eV. While the electrochemical data suggest a weak intramolecular interaction between the fluorenyl moieties, the emission spectra recorded in solution show no significant differences between the **SiFln** molecules.

Photoluminescence spectra from thin films of **SiFln** were measured at both room temperature and 77 K (Figures 3c and S4). The emission properties of the neat films are markedly different from those of the isolated molecules. Three different types of emission can be resolved in the spectra from the films. High energy bands are observed between 300−400 nm (strongest for **SiFl2** and **SiFl3**) and assigned to singlet emission from the isolated fluorenyl group. A strong, featureless band is also observed between 400−500 nm. This blue emission line has a lifetime of 2.5 ns and gives a PL efficiency of 0.14. This transition is significantly red-shifted from spectra recorded in dilute solution and is thus assigned to singlet emission from aggregate states. At low temperature, a new band appears between 500−600 nm (Figure 3c). This low energy band has a long lifetime (~700−800 ms), which leads us to assign the feature to triplet emission from the aggregates in the **SiFln** films.

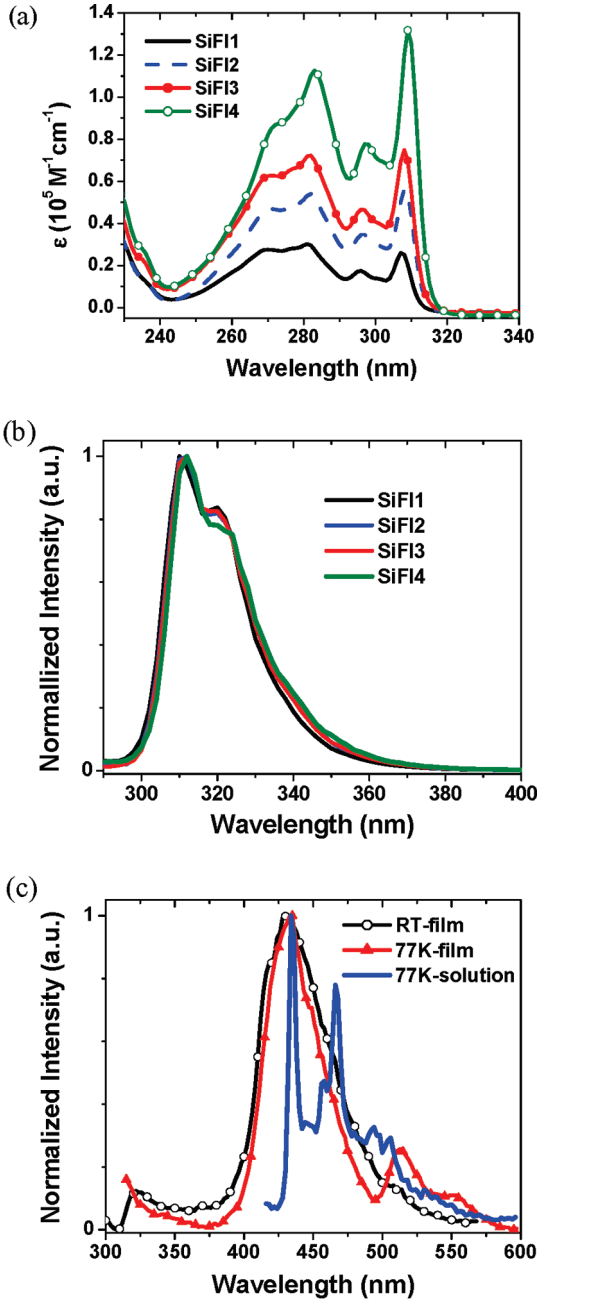

Figure 3. (a) Absorption and (b) emission spectra of **SiFln** in CH_2Cl_2 solution. (c) Emission spectra from neat films of **SiFl4** recorded at room temperature (RT) and 77 K along with the phosphorescence spectrum of **SiFl4** measured in 2-MeTHF solution at 77 K.

OLED Studies. The charge transport properties of the **SiFln** compounds were investigated using three- and four-layer OLEDs. The structures used were ITO/NPD

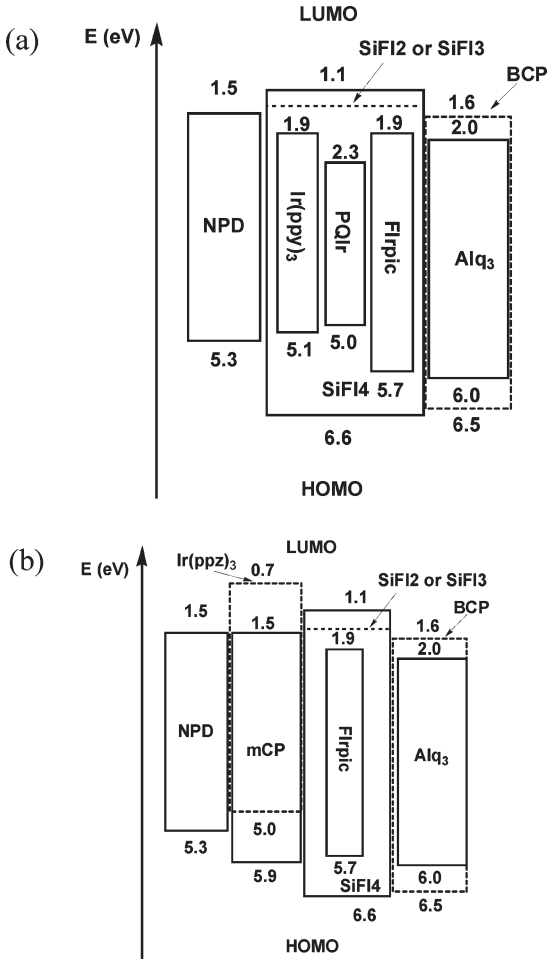

Figure 4. Energy diagrams of the fabricated OLED devices. The scheme for device III shows the energies for three different dopants. Devices utilize only a single dopant, not mixtures. (a) Device I: ITO/NPD (40 nm)/**SiFln** (20 nm) (n = 2, 3, 4)/Alq_3 (20 nm)/LiF (1 nm)/Al (100 nm). Device III: ITO/NPD (40 nm)/dopant: **SiFl4** (20 nm), (dopant = PQIr, $Ir(ppy)_3$, or FIrpic)/BCP (40 nm)/LiF (1 nm)/Al (100 nm). (b) Device II: ITO/NPD (30 nm)/mCP (10 nm)/**SiFln** (20 nm) (n = 2, 3, 4)/Alq_3 (20 nm)/LiF (1 nm)/Al (100 nm). Device IV: ITO/NPD (30 nm)/mCP (10 nm)/FIrpic: **SiFl4** (20 nm)/BCP (40 nm)/LiF (1 nm)/Al (100 nm). Device V: ITO/NPD (30 nm)/$Ir(ppz)_3$ (10 nm)/FIrpic: **SiFl4** (20 nm)/BCP (40 nm)/LiF (1 nm)/Al (100 nm).

(40 nm)/**SiFln** (20 nm, n = 2, 3, 4)/Alq_3 (20 nm)/LiF (1 nm)/Al (100 nm) (device I), and ITO/NPD (30 nm)/mCP (10 nm)/**SiFln** (20 nm, n = 2, 3, 4)/Alq_3 (20 nm)/LiF (1 nm)/Al (100 nm) (device II). The low sublimation temperature of **SiFl1** precluded OLED studies using this material. Wu et al. showed that oligofluorenes have ambipolar carrier conduction properties,[14−17] suggesting that the location of charge build-up and recombination in these devices should be controlled by injection barriers at the HTL and ETL interfaces. Figure 4 shows the relative HOMO/LUMO energies of the materials used in the devices. The LUMO of Alq_3 (2.0 eV) lies below that of the fluorenylsilanes (1.1−1.4 eV) presenting a 0.6−0.9 eV barrier for injecting electrons from Alq_3 into **SiFln**. The HOMO of NPD (5.3 eV) is 1.3 eV higher than that of the fluorenylsilanes (6.6 eV), giving a much higher barrier to the hole injection into **SiFln** than for electron injection in device I (Figure 4a). Thus, for device I we do not expect to see emission from Alq_3. OLEDs with device structure I using

Table 3. Performance of Undoped Devices I and II

device	n	EL maxima (nm)	turn-on voltage[a] (V)	maximum luminance (cd/m^2)	$\eta_{ext,\ max}$ (%)
I	**2**	432	7.2	464 (at 15 V)	0.3
	3	432	4.7	648 (at 13 V)	0.3
	4	432	4.5	392 (at 15 V)	0.3
II	**2**	432, 516	4.5	3945 (at 15 V)	0.4
	3	432, 516	4.5	3984 (at 13 V)	0.5
	4	432, 516	3.9	5911 (at 14 V)	0.5
	UGH2	432	8.7	385 (at 15 V)	0.2

[a] Determined at a luminance of 0.1 cd/m^2.

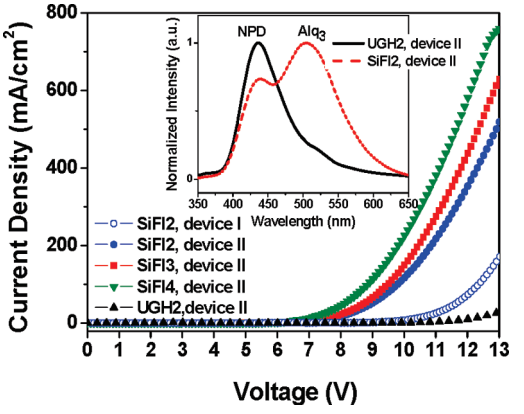

Figure 5. Current density vs voltage plots of devices I and II. The inset spectrum shows the EL spectra measured at 12 V for the UGH2 and **SiFl2** devices.

SiFl2, **SiFl3**, and **SiFl4** give only blue emission (λ_{max} = 432 nm, from either NPD or **SiFln**) at voltages ranging from 7 to 15 V, as expected based on the high barrier to the hole injection into the fluorenylsilane layer. The turn-on voltages (at 0.1 cd/m^2) also decrease as the number of fluorenyl groups in the molecule increase. While the **SiFl2** device turns on at 7.2 V, the **SiFl3** and **SiFl4** devices turn on at 4.7 and 4.5 V, respectively, as seen in Table 3. Presumably, the increased fluorene content in the **SiFl3** and **SiFl4** layers increases the density of charge conducting states at NPD/**SiFln** interface and, thus, lowers the potential for charge injection into the film.

The large barrier for hole injection into the **SiFln** film can be mitigated by inserting a thin layer of mCP between the NPD and **SiFln** materials (device structure II). The HOMO energy of the mCP layer (5.9 eV) is intermediate between that of NPD and **SiFln**, thereby creating an energetic "step" to facilitate hole injection into **SiFln** (Figure 4b). A closely related device architecture has been previously employed to enhance hole injection in OLEDs.[36] OLEDs with device structure II have turn-on voltages of 3.9−4.5 V (Table 3). For devices made using the same fluorenylsilane material, holes are injected more efficiently with an mCP layer present than without. For example, the current density for device I using **SiFl2** was 171 mA/cm^2 at 13 V, while for device structure II the measured value was nearly three times greater at the same bias. The current densities of the devices

(36) Loy, D. E.; Koene, B. E.; Thompson, M. E. *Adv. Funct. Mater.* **2002**, *12*, 245.

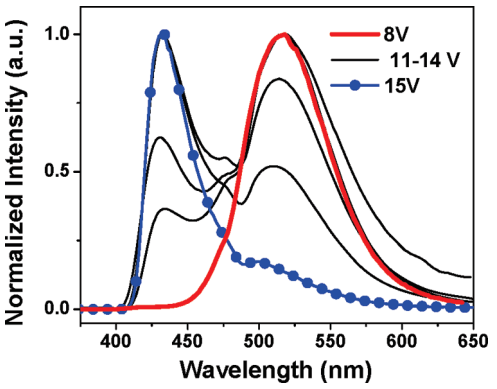

Figure 6. Voltage dependence of the EL spectra of the device: ITO/NPD (30 nm)/mCP (10 nm)/**SiFl4** (20 nm)/Alq_3 (20 nm)/LiF (1 nm)/Al (100 nm). As the voltage increases from 8 to 15 V, the peak at 432 nm increases, while the peak at 516 nm decreases.

with structure II also increase with increasing fluorene content in the **SiFln** layer (Figure 5), which implies that the fluorenyl group is the dominant charge carrying moiety in the film.

The **SiFln** layer exhibits ambipolar charge transport characteristics based on the voltage dependence of the EL spectra. The emission spectra measured for device ITO/NPD/mCP/**SiFl4**/Alq_3/LiF/Al are shown in Figure 6. Pure Alq_3 emission was observed at a low voltage (8 V) indicating that recombination takes place at or near the Alq_3 layer. As the voltage increases, the contribution of blue emission increases, thus more charge recombination takes place away from the Alq_3 interface. At 15 V, the electroluminescence (EL) spectrum is dominated by blue emission.

We also compared the charge transport properties of the **SiFln** to another arylsilane, 1,4-bis(triphenylsilyl)-benzene (UGH2),[11] by fabricating an analogous device: ITO/NPD/mCP/UGH2/Alq_3/LiF/Al. As shown in Figure 5, all of the devices using **SiFln** give markedly higher current densities at a given voltage than the related UGH2 device. This is likely due to greater charge carrier mobilities and the shallower HOMO of **SiFln** (6.6 eV) relative to UGH2 (7.2 eV). A comparison between EL spectra at 12 V from OLEDs using either **SiFl2** or UGH2 is shown in Figure 5, inset. The **SiFl2** molecule is shown for this comparison since it has both a size and molecular density close to that of UGH2. Very little Alq_3 emission is observed from the device made with UGH2 . Even with the presence of an mCP layer, a large energy barrier prevents hole injection from the mCP into the UGH2 layer. On the other hand, the EL spectrum from the device using **SiFl2** displays a substantial contribution from Alq_3, which indicates improved hole injection from the HTL due to the relatively high HOMO level of the **SiFl2** layer.

Green and red phosphorescent devices were fabricated using **SiFl4** as the host for emissive dopants in heterojunction devices. The structure used for these devices (device III) was ITO/NPD (40 nm)/dopant: **SiFl4** (20 nm)/BCP (40 nm)/LiF (1 nm)/Al (100 nm), where BCP = 2,9-dimethyl-4,7-diphenyl-1,10-phenanthroline. The *fac*-tris(2-phenylpyridyl)iridium ($Ir(ppy)_3$, 6%) and

Table 4. Performance of Phosphorescent Devices III, IV, and V

device	dopant	EL maxima (nm)	turn-on voltage[a] (V)	maximum luminance (cd/m^2)	$\eta_{ext,\,max}$ (%)
III	$Ir(ppy)_3$	510	3.0	9514 (at 13 V)	8
	PQIr	595	3.2	4814 (at 14 V)	8
	FIrpic	432	4.2	2605 (at 15 V)	0.4
VI	FIrpic	432(strong), 468	3.9	3053 (at 14 V)	2
V	FIrpic	468	4.4	458 (at 15 V)	3

[a] Determined at a luminance of 0.1 cd/m^2.

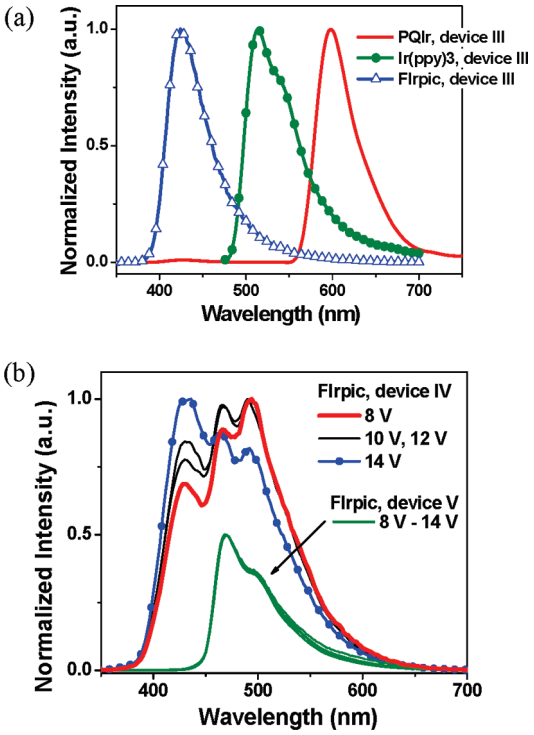

Figure 7. EL spectra of (a) devices III and (b) device IV and device V. In device IV, the peak at 432 nm increases, while the peaks at 468 and 492 nm decrease from 8 to 14 V. The EL spectra of device V do not change from 8 to 14 V.

bis(2-phenylquinolyl)iridium acetylacetonate (PQIr, 6%) complexes were used as dopants for the green and red OLEDs, respectively. Table 4 summarizes the performance of all these doped devices. The HOMO energy levels of $Ir(ppy)_3$ and PQIr are well above those of the fluorenylsilanes and close to that of NPD, which facilitates hole injection into the emissive layer and eliminates the need for a mCP hole injection layer (Figure 4a). Pure dopant emission was observed for both the green and red emissive devices (Figure 7a). These two devices turn on at roughly 3.0 V, and the highest quantum efficiencies (8%) were measured for both devices at a current density of 0.01 mA/cm^2 (Figure S5b).

The triplet energies of the **SiFln** molecules (2.9 eV) are greater than the triplet energies of the blue phosphorescent dopants, such as bis[(4,6-difluorophenyl)pyridyl]-iridium picolinate (FIrpic, E_T = 2.65 eV), making the fluorenylsilanes potential hosts for blue phosphorescent emitters. However, the low triplet energy of the aggregate states in film (Figure 3c) could compromise the performance of the OLEDs. To examine this possibility, blue

phosphorescent devices using device structure III were prepared using FIrpic (10 wt %) as the emissive dopant. No emission from FIrpic was observed in these devices, suggesting that a sufficiently large barrier to hole injection is present that limits charge recombination to the HTL layer. FIrpic has a markedly deeper HOMO energy than either $Ir(ppy)_3$ or PQIr (Figure 4a). In order to promote hole injection, an OLED with FIrpic was also prepared using device structure IV (ITO/NPD (30 nm)/mCP (10 nm)/FIrpic: **SiFl4** (10%, 20 nm)/BCP (40 nm)/LiF (1 nm)/Al (100 nm)), in which a mCP layer is inserted between the NPD layer and the EML (Figure 4b). Emission from FIrpic can be observed for this device (Figure 7b), suggesting that recombination takes place in both the HTL and the intended emissive layer (FIrpic: **SiFl4**). The EL spectrum was observed to be strongly voltage dependent (Figure 7b), with predominant FIrpic emission at low voltage (8 V) and predominant emission from the HTL layer at high voltage (14 V). The significant emissive contribution from HTL layer leads to a relatively low efficiency in this device, peaking at roughly 2% (Table 4).

The *fac*-tris(1-phenylpyrazolyl)iridium complex, $Ir(ppz)_3$, has been shown to be both a good hole injecting and electron blocking material.[9,37] Substituting $Ir(ppz)_3$ in place of mCP is expected to prevent electron leakage into the HTL layer and give pure dopant emission. Device V, i.e. ITO/NPD (30 nm)/$Ir(ppz)_3$ (10 nm)/FIrpic: **SiFl4** (10%, 20 nm)/BCP (40 nm)/LiF (1 nm)/Al (100 nm), was prepared to explore the effect of $Ir(ppz)_3$ incorporation on device performance (Figure 4b). As expected, device V gives only FIrpic emission (λ_{max} = 468 nm) at all voltages examined (8−14 V) (Figure 7b). While this device gives emission exclusively from the phosphorescent dopant, the peak efficiency (3% at 3 V) is still well below values achieved for the OLEDs using green and red dopants (Table 4). The poor performance of the blue devices could be due to the presence of host aggregates. As mentioned previously, the aggregates have triplet state energies (510 nm, 2.43 eV) that are much lower than that of FIrpic. While the energy of triplet state of the aggregates is too high to quench either the green or red dopants, the value is low enough to adversely affect the efficiency of the devices doped with FIrpic.

(37) Tamayo, A. B.; Alleyne, B. D.; Djurovich, P. I.; Lamansky, S.; Tsyba, I.; Ho, N. N.; Bau, R.; Thompson, M. E. *J. Am. Chem. Soc.* **2003**, *125*, 7377.

Summary

We have designed and synthesized four fluorenylsilanes with varying number of fluorenyl moieties, ranging from one to four. These materials give high glass transition temperatures (for n = 2, 3, and 4) and reversible reductions, making them good host candidates for OLED applications. Systematic studies including electrochemistry, photophysics, and OLED device studies have been performed to investigate the charge transport abilities of these molecules. Device data suggest the fluorenylsilanes have ambipolar characteristics. Their large HOMO−LUMO gap and the high triplet energy confine excitons to green and red phosphorescent emitters in doped OLEDs. High external quantum efficiencies were observed for the green and red phosphorescent devices fabricated with $Ir(ppy)_3$ and PQIr doped into **SiFl4**. We also found that these molecules could be utilized as host materials for blue OLEDs. However, the presence of aggregated states with low triplet energies in neat films of **SiFl4** limits the performance of the latter devices.

Acknowledgment. The authors acknowledge financial support of this work from Universal Display Corporation. We also thank Thin Film Devices Inc. for the indium tin oxide substrates used in this work.

Supporting Information Available: Differential scanning calorimetric (DSC) thermograms of **SiFln**; differential pulse voltammetric (DPV) traces from electrochemical reduction of **SiFln**; HOMO and LUMO orbitals of **SiFln** and triplet spin density surfaces of **SiFl1−3** calculated using DFT; emission spectra from neat films of **SiFln** at room temperature and 77 K; and the current density vs voltage and quantum efficiency vs current density of devices III, IV, and V. This material is available free of charge via the Internet at http://pubs.acs.org.